Biocompatibility of Multi-Imaging Engineered Mesoporous Silica Nanoparticles: *In Vitro* and Adult and Fetal *In Vivo* Studies

Sean Sweeney[1] PhD, Andrea Adamcakova-Dodd[2] PhD,
Peter S. Thorne[3] PhD, and Jose G. Assouline[4,*] PhD

[1] NanoMedTrix Post-Doctoral Research Associate, Department of Biomedical Engineering, University of Iowa,
229 Engineering Research Facility, Iowa City, IA 52242
[2] Environmental Health Sciences Research Center Department of Occupational and Environmental Health, University of Iowa,
170 Institute for Rural and Environmental Health, Coralville, IA 52241
[3] Occupational and Environmental Health, University of Iowa, S341A College of Public Health Building,
145 N. Riverside Dr., Iowa City, IA 52242
[4] NanoMedTrix, Department of Biomedical Engineering, University of Iowa, 227 Engineering Research Facility, Iowa City, IA 52242

Despite potentially serious adverse effects of engineered nanoparticles on maternal health and fetal development, little is known about their transport across the placenta. Human and animal studies are primarily limited to *ex vivo* approaches; the lack of a real-time, minimally invasive tool to study transplacental transport is clear. We have developed functionalized mesoporous silica nanoparticles (MSN) for use in magnetic resonance, ultrasound, and fluorescent imaging. This material is designed as a model for, or a carrier of, environmental toxicants, allowing for *in vivo* evaluation. To establish a baseline of biocompatibility, we present data describing MSN tolerance using *in vitro* and *in vivo* models. In cultured cells, MSN were tolerated to a dose of 125 μg/mL with minimal effect on viability and doubling time. For the 42 day duration of the study, none of the mice exhibited behaviors usually indicative of distress (lethargy, anemia, loss of appetite, etc.). In gravid mice, the body and organ weights of MSN-exposed dams were equivalent to those of control dams. Embryos exposed to MSN during early gestation were underweight by a small degree, while embryos exposed during late gestation were of a slightly larger weight. The rate of spontaneous fetal resorptions were equivalent in exposed and control mice. Maternal livers and sera were screened for a complement of cytokines/chemokines and reactive oxygen/nitrogen species (ROS/RNS). Only granulocyte-colony stimulating factor was elevated in mice exposed to MSN during late gestation, while ROS/RNS levels were elevated in mice exposed during early/mid gestation. These findings may usher future experiments investigating environmental toxicants using real-time assessment of transport across the placenta.

KEYWORDS: *Mesoporous Silica Nanoparticles, Placenta, Maternal-Fetal Medicine, Biocompatibility, Magnetic Resonance Imaging, Reactive Oxygen Species.*

INTRODUCTION

Given recent increases in production of consumer goods with nanomaterial components, the likelihood of environmental exposure to engineered nanoparticles (NPs) is on the rise. Mesoporous silica nanoparticles (MSN) are becoming more widespread in both industrial[1] and medical applications.[2,3] MSN and other metal oxides are of interest to human health because they often have unique properties not present in their bulk state. For instance, the extremely high surface area-to-volume ratio of MSN make them favorable for drug delivery applications[3,4] while also providing a high energy surface that may generate inflammation. Thus, there is a need to evaluate the toxicology of these engineered materials, preferably prior to their widespread use.

In order for toxicity to occur, the NPs must cross one or more of the biological barriers. Many NPs are readily

absorbed percutaneously,[5] while others are inhaled.[6] Once NPs have entered the bloodstream, they may encounter an additional barrier in the placenta.[7–10] Despite the susceptibility of pregnant women and developing fetuses to environmental particulate contamination, relatively little is known about the effects of NP exposure, and specifically MSN during pregnancy on either mother or fetus.

Inhalation of NPs during pregnancy may induce acute placental inflammation[11] associated with inadequate placental perfusion and a decrease in transplacental nutrient exchange.[12] Several studies found that inhaled or injected NPs enter the systemic circulation and can migrate to kidneys, liver, heart, brain and bone.[13, 14] Silica NPs with a diameter < 100 nm were absorbed through the nasal cavity after intranasal instillation and distributed into liver and brain.[6] There is a possibility that inhaled or injected NPs can reach the placenta or even pass through the placenta to the fetus. However, few studies have investigated transport of nanomaterials to the placenta and their effects on the fetus.[7, 8] An *ex vivo* study of the barrier capacity of human placenta found that polystyrene particles (50–300 nm) were taken up by the placenta and were able to cross the placental barrier,[10] while an *in vivo* study in mice showed that quantum dots crossed the placental barrier.[8] There might also be indirect effects of prenatal inhalation exposure to NPs on the developing fetus: injection of chromium cobalt NPs in mice during pregnancy led to a ∼2.5-fold increase in DNA damage in neonatal blood, even though there were no other pathologic changes observed.[15]

Modes of particle exposure other than inhalation are important as well, including translocation of NPs to fetus and the effects of NPs on the developing fetus after i.v.[15, 16] or subcutaneous[13] administration. Silica and titanium dioxide NPs (with primary diameters of 70 and 35 nm, respectively) were found in the placenta, fetal liver and brain after i.v. administration.[16] Regardless of exposure model, techniques for evaluating exposure are similar, typically involving assays of whole blood for the particle or related metabolites, or microscopy (a combination of light, confocal, and/or electron microscopy) on sections from tissues of interest. Whole blood assays generate useful information about the amount of particles in circulation at any given time, without terminating the experiment. However, these assays cannot show in which tissue the particles are accumulating. Conversely, histopathological assays can reveal the accumulation of particles in specific organs, but require necropsy. In addition, the use of electron microscopy to detect NPs in tissues is time-consuming and costly, and some forms of NPs are more difficult to detect than others. Thus, there exists an opportunity to improve upon this paradigm. If nanoparticle-based therapeutic interventions are considered for maternal-fetal health, it is appropriate to determine the limiting factors, best presentation and timeliness of the exposure.

Our group has developed a novel nanoparticle based on mesoporous silica that has been functionalized for multimodal imaging, using a combination of fluorescence, MRI, CT and/or ultrasound. The particle has a mean diameter of 50 nm in its simplest configuration to 187 nm in its largest form (depending on the particle composition) and a hexagonal array of pores 2.4 nm in diameter. Due to their structural properties (particle size, morphology, and porosity), MSN are very versatile tools for many applications such as bioimaging,[17, 18] drug release,[3, 19] environmental remediation[1] (for removing heavy metals from water), and development of sensors and energy transfer devices.[20] Although others have developed MSN for use in bioimaging, our MSN are the first with this configuration. We hypothesize that MSN may be used to provide additional information about *in vivo* nanoparticle trafficking in a way that does not necessitate microscopy or terminal experiments. Rather, particles are tracked non-invasively in a living animal over time, and when the experiment is terminated, fluorescent microscopy is used to determine particle accumulation. In these initial studies, our twofold goals are to demonstrate the tolerance of cells in culture and mice to MSN and the ability to track cells *in vivo* non-invasively. In addition, these studies will pave the way for future efforts to track the transplacental transport of nanoparticles in a gravid mouse model and non-invasive evaluation of fetal life.

MATERIALS AND METHODS
Particle Synthesis and Characterization

Mesoporous silica nanoparticles functionalized with Gd_2O_3 and fluorophore (fluorescein or tetramethyl rhodamine isothiocyanate) (FITC-Gd_2O_3-MSN) were manufactured following a previously reported synthesis[21] and stored at room temperature. An aliquot of this synthesis, which yielded over 1 gram of dried MSN, was further functionalized with trifluoropropyl moieties by grafting (3, 3, 3) trifluoropropyl trimethoxysilane onto the surface under reflux with toluene. Similarly, MSN with fluorophore only (FITC-MSN) and MSN with other metals (Fe_3O_4-FITC-MSN; Bi_2O_3-FITC-MSN; Au-FITC-MSN) were synthesized. Size and morphology homogeneity were characterized by X-ray diffraction (XRD), using a Rigaku Ultima IV diffractometer, nitrogen sorption analysis in a Micromeritics ASAP 2020 surface area and porosity analyzer using the Brunauer-Emmett-Teller (BET) equation to calculate surface area and pore volume and the Barrett-Joyner-Halenda (BJH) equation to calculate the pore size distribution. Dynamic light scattering (DLS) was used to obtain particle size distribution and zeta potential data, using the Malvern Zetasizer Nano ZS instrument (University of Iowa, Department of Chemistry). The materials were also visualized by transmission electron microscopy (TEM) by supporting samples on copper grids in a JEOL JEM 1230 microscope operating at 40–120 kV

(University of Iowa, Central Microscopy Research Facility).

In Vitro Biocompatibility

In order to evaluate the tolerance of cultured cells to MSN, initial experiments were conducted to determine the highest dose tolerated. Cells tested include human bone marrow-derived mesenchymal stem cells (hMSCs) and murine induced pluripotent stem cells (iPSCs), MB49 murine bladder cancer cells, NIH3T3 murine embryonic fibroblasts, and H4IIE rat hepatoma cells (obtained from ATCC). Cells were seeded at 10^5 cells/cm^2 in a 24-well tissue culture plate, and exposed to MSN species at concentrations ranging from 0 to 1000 μg/mL. Subsequent experiments were carried out using between 100 and 125 μg/mL concentrations. Stock solutions of MSN species were created by suspending 5 mg MSN in 500 μL Dulbecco's phosphate buffered saline (DPBS, Life Technologies, Madison, WI). The suspension was sonicated using an ultrasonic water bath operating at 42 kHz and 35 W for 5 min, then 100 μg MSNs were added to each of the wells of mesenchymal cells seeded previously. DLS testing indicated that a minimum of 5 minutes of sonication under these conditions ensured maximal dispersion of particles. Further confirmation of dispersibility was obtained by performing random sampling of the aliquots following sonication regimens. To visualize particle uptake by cells in real-time, the 6-well plate containing FITC-MSN was imaged using the Olympus® IX70 fluorescence microscope at 494 nm with an attached DP70 digital camera and software. Images were obtained at 1, 7 and 26 h following addition of the particles. After 27 h, particles that were not engulfed were rinsed from the culture using DPBS, and images were acquired for 10 additional days. Non-adherent iPSCs were characterized for viability using trypan blue exclusion dye and a hemacytometer, and labeling efficiency was measured using flow cytometry. Cells were washed with DPBS and fixed with 2% Paraformaldehyde prior to acquisition through a BD LSR II Violet Instrument (Becton Dickinson, Franklin Lakes, NJ). The collected data were analyzed with FlowJo software (FlowJo, Ashland, OR).

In Vivo Biocompatibility

The *in vivo* tolerance of intravenously injected MSN was assessed in two different mouse models: (1) mouse model for bone marrow transplant and (2) gravid mouse model. All animals were purchased from Jackson Laboratories (Bar Harbor, ME). In a mouse model for bone marrow transplant, 129 SvJ mice (females, on Balb/c background) were housed at the vivarium located in the Veteran Affairs Medical Center, Iowa City, IA. In a gravid mouse model, C57Bl/6 (males 6 wks old and females 8 wks old) were housed in an AAALAC-accredited vivarium, in polypropylene, fiber-covered cages in HEPA-filtered Thoren caging units (Hazelton, PA). They were

acclimatized for 10 days after their arrival and were maintained on a 12-hr light/dark cycle with *ad libitum* access to food and water. To establish timed pregnancies, 2 nulliparous females were mated with one mature male for three days. The presence of a vaginal plug was assessed each morning and if found, this day was considered as gestation day (GD) 1. All procedures were approved by the Institutional Animal Care and Use Committee (IACUC) and performed according to NIH guidelines.

Mode of Injection

In bone marrow transplant studies, adult mice were irradiated at least 24 h prior to injection with 700–800 cGy of cesium split in two doses spaced 4 h apart. In this study, 4-wk-old mice received an injection of $7.2*10^6$ labeled CCE-hematopoietic progenitor cells (HPCs, a mouse embryonic stem cell line derived from 129/SvJ mice), plus $5*10^5$ cells from the bone marrow of a third mouse to enhance engraftment of the HPC cells, retro-orbital to the left eye. MRI images were acquired for up to 22 days; animals remained in observation for adverse reactions to the cells or particles for up to 6 weeks. Additional 129 SvJ mice were injected retro-orbitally with 1 mg free PEG-CF$_3$-TRITC-Gd$_2$O$_3$-MSN in 0.1 mL saline. Mice were subsequently scanned in the Varian® Unity/INOVA 4.7 T small animal MRI scanner using a 25 mm gradient coil. Before and at several time points after retro-orbital injection of labeled cells, the mouse was anesthetized with isoflurane (3% induction, 1.5% maintenance) and scanned using fast spin echo (FSE) sequences (typical repetition time 2100 ms, echo time 15 ms with an echo train length of 8 and 5 averages per scan). Three scans were interlaced to yield images 256×512 pixels with 45 slices, and a voxel size of $156 \times 156 \times 500$ μm. Each of the 3 sequences had a scan time of 8 min, and an additional T2*-weighted gradient echo scan was done for a total scan time of about 45 min per mouse. In a gravid mouse model, mice were given intravenous injections of 1 mg PEG-CF$_3$-TRITC-Gd$_2$O$_3$-MSN in 0.1 mL DPBS via tail vein at varying stages in gestation: early/mid (7–9 days) and late (15–17 days), with other mice receiving sham (DPBS) injections. The gravid mice were scanned in MRI, and the intensity of the maternal liver, placenta, and fetal liver, heart, and brain measured. Reconstructed images were saved as 16 bit TIF image stacks, which were opened with MIPAV software for analysis. Volumes of interest (VOIs) were either manually drawn or semi-automatically selected using the "levelset VOI" tool. Images were normalized to one another using a volume of fat adjacent to the kidneys.

Cytokine/Chemokine, ROS/RNS and Biochemistry Parameters Analyses

After scanning, the mice were euthanized by overdose of isoflurane, whole blood was collected for later serum or plasma analyses and the uteri were excised.

Maternal organ weights, litter size/number of spontaneous resorptions, placenta weight, and average weight and length of each pup were measured. Whole blood collected for serum was kept at room temperature after collection for about 2–3 hrs, then centrifuged at $1500\times$ g for 10 min. Serum was then aliquoted and stored at -80 °C until analyzed. Cytokines/chemokines (interleukin [IL]-1α, IL-1β, IL-2, IL-3, IL-4, IL-5, IL-6, IL-10, IL-12/p40, IL-12/p70, IL13, IL-17, eotaxin, granulocyte-colony stimulating factor [G-CSF], granulocyte/macrophage-colony stimulating factor [GM-CSF], interferon-gamma [IFN-γ], keratinocyte chemoattractant [KC], monocyte chemoattractant protein-1 [MCP-1], macrophage inflammatory protein-1α [MIP-1α], macrophage inflammatory protein-1β [MIP-1β], RANTES, tumor necrosis factor-α [TNF-α]) in serum of dams were analyzed using a multiplex magnetic bead assay (Luminex 100, Bio-Rad Laboratories, Inc.). Free radical species were measured in maternal serum using Oxiselect *in vitro* ROS/RNS assay kits (Cell Biolabs, Inc.). Oxidation reaction of ROS samples with DCFH probe after 45 min incubation was measured fluorometrically at 480 nm excitation/530 nm emission (Spectra-Max M5, Molecular Devices). Whole blood collected for plasma analyses was collected in lithium heparin plasma separator microtainer tubes and centrifuged at $1500\times$ g for 10 min. The following biochemistry parameters were measured in plasma: albumin, alkaline phosphatase (ALP), alanine transaminase (ALT), aspartate transaminase (AST), blood urea nitrogen (BUN), calcium (Ca), chloride (Cl), cholesterol, creatinine, γ-glutamyl transpeptidase (GGT), globulin, glucose, phosphorus (P), potassium (K), sodium (Na), total bilirubin and total protein (Catalyst DX Chemistry Analyzer, IDEXX, Westbrook, ME).

Histopathological Evaluation

Maternal livers and kidneys, as well as whole embryos and placentas, were fixed in 10% formalin and embedded in paraffin, then serially sectioned with a thickness of 4 μm. Sections were mounted on glass slides and stained with hematoxylin/eosin, while adjacent sections were left unstained for fluorescent microscopy. Histopathology of the livers and kidneys was evaluated by a board-certified veterinary pathologist (Comparative Pathology Laboratory, University of Iowa).

Statistical Analysis

Experimental group sizes were determined from calculations of statistical power based on relevant past experiments. We typically study the number of animals needed in each group to yield a statistical power of 90% based upon the means and standard errors of the outcome variables assuming a two-sided test of the null hypothesis accepting a 1% level of significance. For studies of nanomaterial-induced effects, calculation of the sample size assuming different means and unequal variances (treating each intervention independently) typically yields a minimum sample size of 6 mice per group in order to have a 90% chance of detecting a significant difference between the groups at the $p < 0.01$ level. To account for mice that do not become pregnant or are sacrificed during the study, we started with 25 mice per group. Statistical significance between pairs of values was determined using Welch's *t*-test for populations of unequal variances, implemented in Microsoft Excel software. Null hypotheses were rejected for *p*-values less than 0.05.

RESULTS
Particle Characterization

To ensure repeatability of synthesis, particles were characterized after each step. The core particle (FITC-Gd_2O_3-MSN) was described previously[21] in a synthesis which yielded over 1 gram of dried powder. Powder XRD analysis confirmed hexagonally arranged mesopores in the diffraction pattern of the Gd_2O_3-MSN as evident by intense d_{100}, and well resolved d_{110} and d_{200} peaks characteristic for MSN. To visualize the size and particle morphology we performed TEM on the FITC-Gd_2O_3-MSN, observing spheroidal particles from 100–300 nm in diameter (Fig. 1(B)). The mesoporous structure was confirmed at higher magnification (Fig. 1(C)). While some overlap of particles occurred in the dry TEM sample, the particles dispersed well in ethanol and aqueous solvents. In deionized water, the FITC-Gd_2O_3-MSN had a ζ-potential of -43.3 mV, becoming -7.12 mV after surface functionalization with trifluoropropyl groups. Further measurement using nitrogen sorption analysis of the FITC-Gd_2O_3-MSN exhibited a Type-IV isotherm (Fig. 1(E)), typical of mesoporous materials, with a Brunauer-Emmett-Teller (BET) surface area of 493 m^2g^{-1}. The average pore diameter for FITC-Gd_2O_3-MSN by Barrett-Joyner-Halenda (BJH) calculation is 38 Å. Using an aliquot of this synthesis, the trifluoropropyl functional groups were grafted onto the surface under reflux to use for ultrasound experiments. Characterization of the size and dispersibility of the fully synthesized CF_3-FITC-Gd_2O_3-MSN was also confirmed by dynamic light scattering (DLS); the median hydrodynamic diameter of the particles was determined to be 227.8 nm (Fig. 1(D)).

In Vitro Biocompatibility

Anchorage dependency is an important element of cell survival. Under adverse conditions, detachment of cells is considered a sign of toxicity.[22] In this study, we demonstrate that at concentrations relevant for imaging, we did not observe a significant cell detachment of anchorage-dependent cells. The external bilayer membrane of adherent and non-adherent cells possess unique properties and respond differently to exogenous toxicants.[23] We investigated the potential cytotoxic effect of non-adherent cells (such as hematopoietic stem cells). In addition, due to recent interest in the intracellular delivery of particles, we
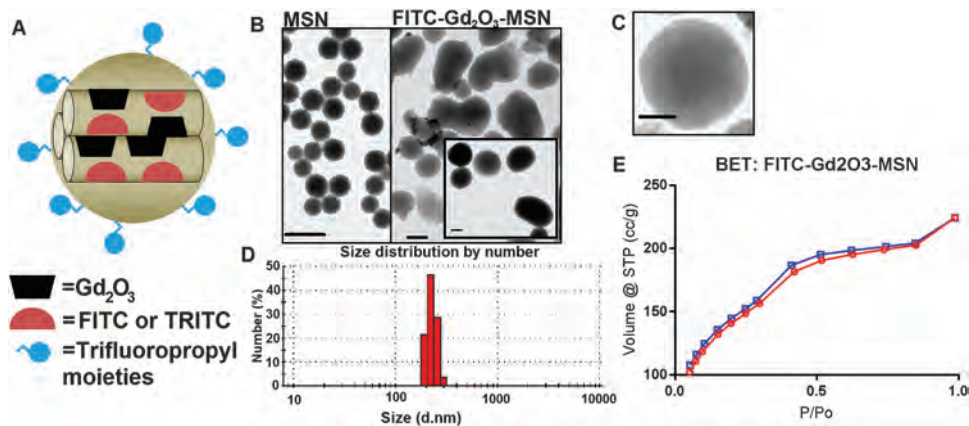
Figure 1. Mesoporous silica nanoparticle (MSN) characterization. (A) Schematic of MSN functionalized with Gd_2O_3, a fluorophore (FITC or TRITC), used for tissue culture studies, and subsequently grafted with trifluoropropyl moieties (CF_3-FITC-Gd_2O_3-MSN) to provide ultrasound contrast for gravid mouse studies. (B–C) Transmission electron micrographs (TEMs) of MSN (left) and FITC-Gd_2O_3-MSN (right, inset, C) indicating particle size and morphology. Scale bars equal 100 nm (B) and 50 nm (C). (D) Dynamic light scattering of the particle in its final configuration (CF_3-FITC-Gd_2O_3-MSN) shows a mean hydrodynamic diameter of 227.8 nm. (E) Nitrogen sorption analysis of FITC-Gd_2O_3-MSN. Adsorption (red) and desorption (blue) isotherms exhibit Type IV isotherms, consistent with mesoporous particles. The Brunauer-Emmett-Teller (BET) surface area was calculated to be 493 m^2g^{-1} and the average pore diameter for FITC-Gd_2O_3-MSN by Barrett-Joyner-Halenda (BJH) calculation is 38 Å.

paid particular attention to cellular translocation, vitality of the cells and maintenance of homeostasis.

For example, we evaluated MSN uptake and viability by anchorage-dependent and non-dependent cells. Because of initial concerns with cell viability when exposed to MSN, initial experiments determined the maximal MSN dose tolerated by the cells relative to controls. A variety of cultured cells (primary and cell lines) were exposed to MSN materials. The MSN species included FITC-MSN, FITC-MSN capped with gold or bismuth Fe_3O_4-FITC-MSN, and Gd_2O_3-TRITC-MSN further functionalized with poly(ethylene glycol). Consistently, cells were highly
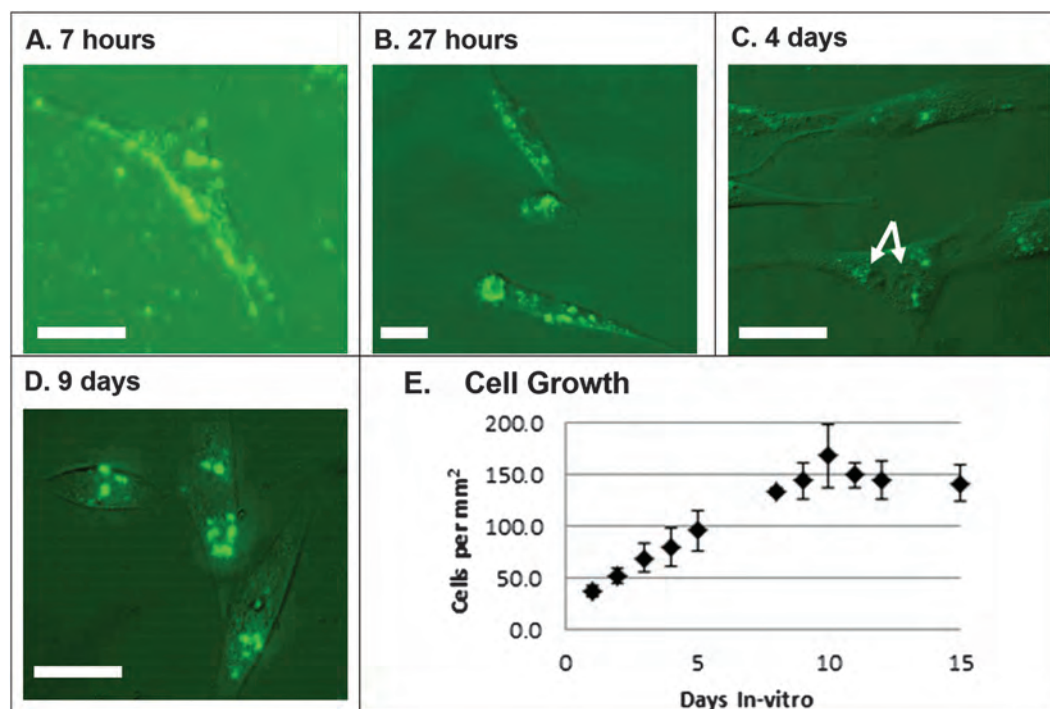

Figure 2. Kinetics of FITC-MSN. (A–D) hMSC were photographed at varying times following addition of 125 μg/mL FITC-MSN to the growth medium. Arrows indicate the daughter nuclei of a mitotic cell. (E) Cells grew in a manner consistent with unlabeled cells, growing to confluence in about 10 days before reaching contact inhibition. Scale bars represent 10 μm; error bars represent standard deviation ($n = 4$ for each data point).

tolerant of concentrations between 100 and 125 μg/mL, while at higher concentrations (about 250 μg/mL) we observe a progressive deleterious effect on the cells. We determined the optimum concentration for use in our experiments to be 125 μg/mL, thus subsequent experiments were carried out using concentrations of this magnitude. One example of uptake and viability measurement, using hMSCs and FITC-MSN, is shown (Figs. 2(A–D)). The hMSCs labeled at this concentration were observed over 16 days, with viable cells counted from multiple micrographs taken of each well. During the exponential growth phase, the cells had a doubling time of about 2 days, comparable with that of non-labeled cells (Fig. 2(E)).[24] Cells reached confluence and underwent contact inhibition at the same rate as non-labeled cells. The proportions of labeled cells and of particles within cells were also measured using fluorescent micrographs.

A MATLAB image processing algorithm was developed to compare the quantity of fluorescent particles inside versus outside the cells at each time point. After 7 hours, 70% of the particles were inside cells, increasing to 95% by 27 hours. Once endocytosed, over 90% of the particles remained in cells for the duration of the study, indicating that exocytosis was minimal. In subsequent experimental days, the particles were seen to integrate the cytoplasm and migrate towards the cell nuclei, likely indicating that they were being compartmentalized, most likely in endoplasmic vesicles.[3] Our observations are consistent with those made by other groups studying similar MSN; in fluorescent confocal images, the particles are co-localized to endosomes, escaping at different times based on surface modifications.[3] Studies employing TEM also describe mesoporous silica within endosomes after 3–4 hours of exposure.[25, 26] Notably, dividing cells were observed at 96 h (Fig. 2(C)), further supporting the notion that the MSN are functionally non-toxic. As evidenced by fluorescence microscopy, we also observed that an approximately equal amount of MSN was detected in the cytoplasmic portion of each daughter cell. The same patterns of internalization, compartmentalization and division appeared with MSN bearing Gd_2O_3, Fe_3O_4, bismuth, and gold caps.

The labeling of non-adherent cell lines such as iPSCs was tested as well. In the first labeling experiment, $1.4 * 10^7$ green fluorescent protein (GFP)$^+$ iPSCs were incubated in an Eppendorf tube with PEG-CF$_3$-FITC-Gd_2O_3-MSN at 125 μg/mL for 4 hours. Flow cytometry, fluorescent microscopy and Wright stains were used to evaluate the cells (Figs. 3(A–D)). The Wright stain revealed the vast majority of cells were mononuclear with a very high ratio of nuclear to cytoplasmic volume, suggestive of a progenitor cell morphology, which suggest that the cells were not adversely affected by their exposure to MSN. Subsequently, a second form of MSN
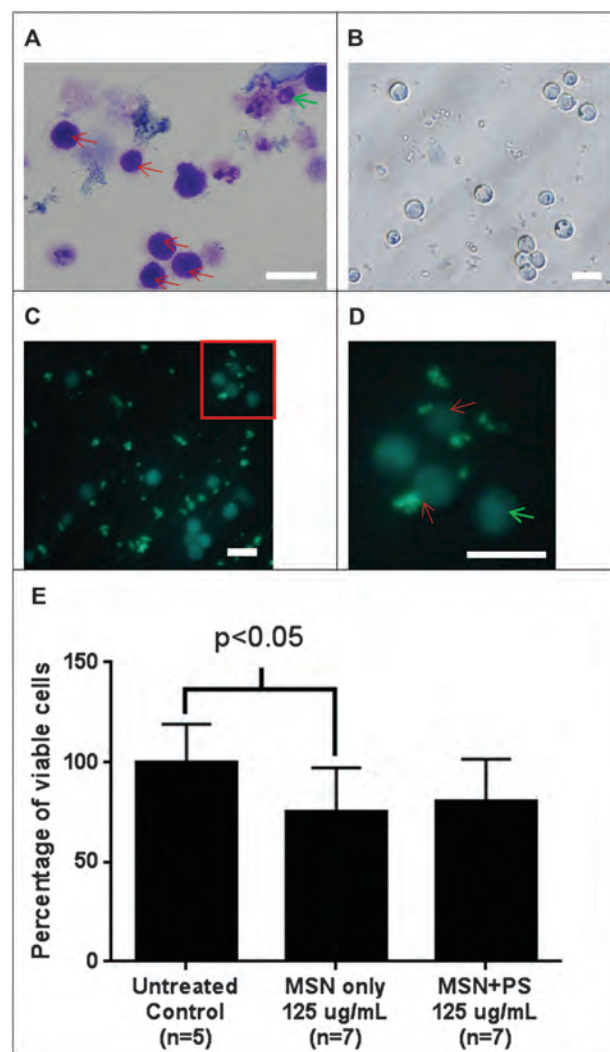

Figure 3. Biocompatibility of non-adherence-dependent cells. Murine iPSCs were exposed to 125 μg/mL MSN for 4 hours. Under Wright stain (A), the vast majority of cells are small with a high ratio of nuclear to cytoplasmic volume, indicative of a progenitor phenotype (red arrows, while a few cells have a lower nuclear to cytoplasmic ratio and granular neutrophilic or eosinophilic cytoplasm (green arrow). iPSCs in bright field (B), showing the same field under GFP fluorescence in (C), with inset (red box) shown in (D). Clear labeling can be observed in some cells (red arrows), while other cells remain non-labeled (green arrow). Supplementing with protamine sulfate (PS) improved iPSC viability (E) relative to cells exposed to MSN alone. Error bars indicate standard deviation. Scale bars represent 20 μm.

with a rhodamine fluorophore (PEG-CF$_3$-TRITC-Gd_2O_3-MSN) was developed, and the cell culture medium was supplemented with protamine sulfate to improve labeling to a maximum of 64%. Viability was reduced to 75% of control cells in MSN alone (Fig. 3(E)), representing a significant decrease ($p < 0.05$); MSN supplemented with protamine sulfate appeared to reduce viability as well, but the difference was not statistically significant.

In Vivo Biocompatibility

Mouse Model for Bone Marrow Transplantation

While *in vitro* experiments test particle tolerance of specific cell lines under highly controlled conditions, ultimately, *in vivo* experiments provide definitive determination of toxicity and systemic responses to exposure to tagged cells or particles alone. In a mouse model of bone marrow transplantation, MRI images were acquired for up to 22 days, though the mice remained in observation for adverse reactions to the cells or particles for up to 6 wk. In total, 11 mice were injected, with only one mouse presenting with stroke-like symptoms and dying shortly after the injection possibly due to aggregation of the particles in the sample injected. Subsequent samples were thoroughly sonicated and vortexed prior to injection. The remaining 10 mice that received sonicated particles and/or cells tolerated the injections quite well for the duration of the experiment, with no appearance of adverse reactions (lethargy, ocular pallor (anemia), loss of appetite, etc.).

All mice were scanned before the injection and again 3 h later, then the following day and 2–3 more times on subsequent days, up to day 22. To measure the maximal hypointensity in MRI caused by the tagged cells, the retro-orbital space was analyzed first. Compared to the "before" scan, considerable hypointensity could be observed in the left eye relative to the right eye in the 3 h scan. Additionally, the total volume of interest measured in this location increased from an average of 5.4 μL at other time points to 8.5 μL. In subsequent scans, the normalized values of the two eyes were virtually identical.

Previously published works discuss renal clearance of nanoparticles with similar sizes and compositions, while larger nanoparticles have been reported to accumulate in the liver.[18, 27–30] In this study, 3 h after injection of particles, the kidneys show an attenuation of the T2-weighted signal, appearing dark relative to the surrounding tissue. This signal persisted through the subsequent 1 day scan. This area (Fig. 4(C)), arrows) is interpreted as most likely
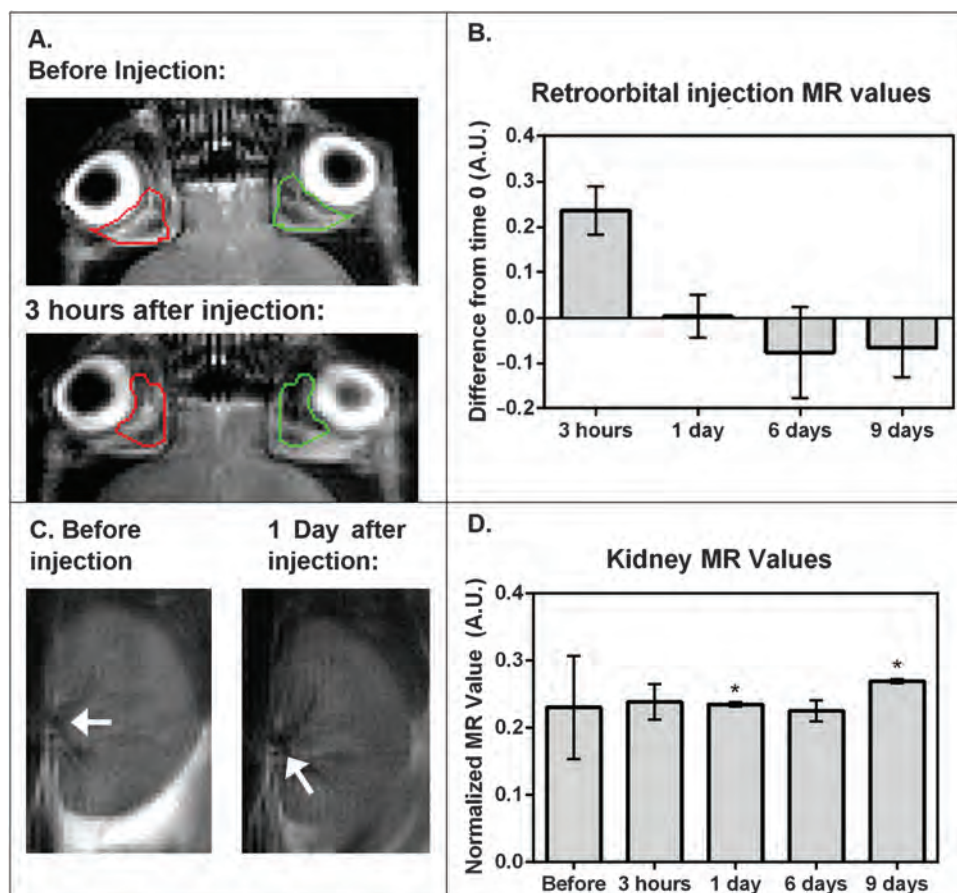

Figure 4. T2-weighted magnetic resonance imaging signal changes are observed following retro-orbital injection of labeled CCE-HPCs. MRI of retro-orbital injection site in a mouse before and at various time points following injection with 7×10^6 labeled CCE-HPC cells (A). Injection was made in the left eye (green region), and the right eye (red region) was used as a control. The plot (B) shows the average normalized signal change relative to the "before" scan, with error bars indicating standard deviation. At 3 h, $p < 0.2$ when compared with zero ($n = 10$). In the kidney (C), the signal in the renal pelvis (arrows) attenuates following injection, diminishing as the experiment continues. In the renal cortex where glomerular filtration takes place, no accumulation of particles was detected. (D) Plot showing the average normalized MR value at each time point for 3 mice with error bars indicating the standard deviation. *comparing the mean at 1 day and 9 days resulted in a significant difference ($p < 0.01$; $n = 10$).

to be renal calyxes/pelvis where formed urine collects. No accumulation of particles is detected in the renal cortex where glomerular filtration takes place.

The T2 signal attenuation was equally distributed in both kidneys, and the volume of interest increased from 898 voxels before the injection to 1449 voxels 3 h after the injection, a 61% increase in volume. Comparing the normalized mean signal at 1 day and 9 days resulted in a significant difference ($p < 0.01$). These findings support the hypothesis that evacuation of MSN occurred through glomerular filtration without detectable accumulation (Fig. 4(C)). Of interest, when compared to retro-orbital injections, the renal clearance was slower (9 days, Fig. 4(A)). This observation supports the interpretation that renal filtration is more expeditious due to the high blood volume and pressure through the organ relative to the retro-orbital space. Free floating MSN (even in its largest form with a mean hydrodynamic diameter of 187 nm) were cleared by the kidneys within 3 days based on the timing of MRI intensity changes (Fig. 4(C)), while larger particles ultimately accumulated in the liver and spleen. No acute renal toxicity was observed, and all exposed mice survived the 42 day duration of the study. Thus the use of MRI to evaluate particle accumulation allows for multiple minimally invasive measurements to be made without the need for dissection, catheterization, or the use of metabolic cages to carry out clearance studies on very small volumes of collected urine.[17, 31]

Gravid Mouse Model

The placenta is one of the most critical barriers protecting the vulnerable developing fetus, yet the parameters for transport across the barrier are not well understood. In the gravid mouse model, 26 animals were injected, with two dying as a result of anesthesia overdose; the remaining animals tolerated the injections for the duration of the experiment. Animals were either injected in early/mid gestation (day 9) or in late gestation (day 14). Maternal weights were recorded at several points during gestation, and normalized relative to their respective day 1 weight (Fig. 5). The average body weight was slightly higher for mice exposed to MSN than for controls, but the difference was not statistically significant for any time point, or for early versus late injection time. Mouse necropsies were performed on GD 17-18, the maternal organs (uteri, livers, lungs, brains, spleen, kidneys, and hearts) were weighed. There were no statistically significant differences in the average weight of each organ between MSN-exposed and control mice (Table I). Spontaneous fetal resorptions were observed in both MSN-exposed (12 resorptions among 7 uteri) and control mice (4 resorptions among 6 uteri). While relatively uncommon in humans, murine spontaneous embryonic resorptions are commonly a result of immune disturbances in the pregnant dam, and significant increases in spontaneous resorptions can be a result of stress.[32, 33] When averaged, the litter sizes for exposed and
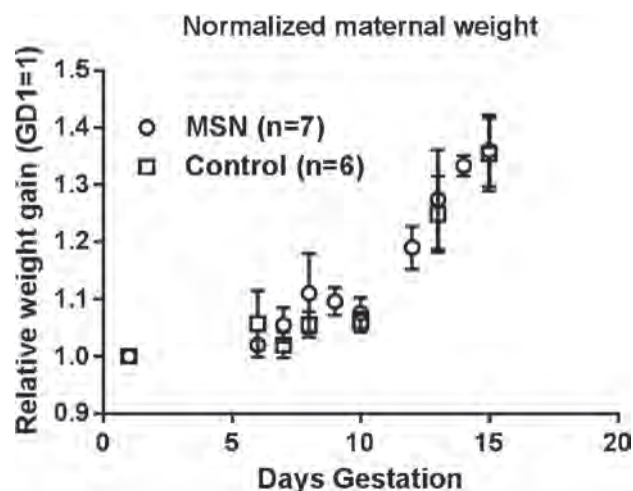

Figure 5. Maternal weights normalized to GD 1 for normal and MSN-exposed mice. Mice were injected with 1 mg PEG-CF$_3$-FITC-Gd$_2$O$_3$-MSN in 0.1 mL DPBS, or with DPBS alone, on GD9. Error bars indicate standard deviations. No significant differences were observed between MSN and control groups.

control mice were not significantly different, regardless of injection time (Table II).

To account for the inherent weight and size difference between laboratory mice, at the time of dissection, the weight of each embryo and its placenta were recorded as well as the dam they came from. Embryos and placentas of MSN-exposed mice injected on GD 9 were slightly underweight relative to controls. However, the absolute weight differences does not take into account the initial weight of the dams prior to pregnancy, which were also slightly lower in the mice eventually exposed to MSN (19.6 ± 1.2 g vs. 20.6 ± 1.5 g). When normalized by dam weight at GD 0, the differences in embryo and placenta weights at GD 9 are not statistically significant (Table II).

In addition, both the placentas and pups of MSN-exposed mice injected on GD 14 were slightly elevated compared to controls. Following normalization calculations taking into account dams' weight at GD 0, the mean embryo weight was only 20 mg larger, and that of the placenta on average was 110 mg larger. These differences were found to be statistically significant ($p < 0.05$). MRI measurements were used to corroborate growth rates based

Table I. Maternal organ weights (grams), GD16, 7 days following MSN exposure.

	Control ($n = 6$)	MSN ($n = 7$)
Uterus with embryos	5.779 ± 0.656	5.014 ± 0.985
Liver	1.491 ± 0.110	1.509 ± 0.117
Brain	0.445 ± 0.025	0.438 ± 0.023
Kidney	0.291 ± 0.021	0.302 ± 0.012
Lungs	0.136 ± 0.020	0.148 ± 0.013
Spleen	0.103 ± 0.020	0.137 ± 0.033
Heart	0.107 ± 0.012	0.109 ± 0.007

Notes: Mean $\pm$ standard deviation; $p > 0.05$ for all comparisons.

Table II. Fetal parameters, GD16.

	Injection day	Control	MSN
Litter size	GD9	7.75 ± 1.26 (n = 4)	7.43 ± 0.53 (n = 7)
Normalized embryo weight (g)	GD9	0.19 ± 0.01 (n = 29)	0.18 ± 0.01 (n = 24)
	GD14	0.17 ± 0.03 (n = 17)	0.20 ± 0.01 (n = 31)*
Normalized placenta weight (g)	GD9	0.43 ± 0.04 (n = 29)	0.23 ± 0.13 (n = 24)
	GD14	0.26 ± 0.08 (n = 17)	0.37 ± 0.04 (n = 31)**
MRI measured fold growth, embryo	GD9	15.32 ± 0.29 (n = 2)	17.32 ± 3.54 (n = 2)
MRI measured fold growth, placenta	GD9	76.8 ± 46.7 (n = 2)	71.8 ± 38.9 (n = 2)

Notes: Mean ± standard deviation; *—$p < 0.05$; **—$p < 0.01$.

Figure 6. Cytokine/chemokine concentrations and reactive oxygen/nitrogen species produced in response to MSN exposure during pregnancy. Gravid mice were exposed to 1 mg PEG-CF$_3$-FITC-Gd$_2$O$_3$-MSN in 0.1 mL DPBS on GD 9 or 14, while negative controls received sham (saline) injections. Necropsies were performed on GD 16. No statistically significant differences were observed in mice exposed on GD9 ($n = 3$) relative to controls ($n = 4$) (A). In mice exposed on GD14 ($n = 4$), only G-CSF was significantly higher in exposed mice than controls ($n = 2$) (B). Mice exposed on GD9, but not GD14, had higher serum ROS/RNS than controls. Error bars indicate standard deviation (**—$p < 0.01$).

on scans acquired at GD 9 and 16 for 2 MSN-exposed mice (16 total embryos) and 2 control mice (15 total embryos). Here, growth was calculated as a fold change of the GD 16 averages relative to the GD 9 averages. No statistically significant differences in placenta and embryo growth were observed.

Concentration of Cytokines/Chemokines, ROS/RNS and Blood Chemistry Parameters

To assess the immune response of the adult mouse to intravenous MSN 23 cytokines/chemokines were assayed. No significant differences of any cytokines or blood parameters were observed for mice exposed to MSN on GD9 relative to controls (Fig. 6(A)). In mice exposed to MSN on GD14, only granulocyte-colony stimulating factor (G-CSF) was produced at a significantly higher level in MSN mice relative to controls (3,300 ± 370 pg/mL vs. 110 ± 16 pg/mL; $p < 0.01$; Fig. 6(B)). The concentration of IL-9 was below the lower limit of detection in all analyzed samples (54 pg/mL).

The ROS/RNS concentrations in maternal sera of mice exposed to MSN on GD 9 were significantly higher than controls (658.3 ± 146.6 nM vs. 117.0 ± 22.1 nM, $p < 0.01$, Fig. 6(A)), but not significantly different from controls in mice exposed on GD 14 (156.2 ± 19.3 nM vs. 144.6 ± 7.7 nM). In the plasma, chloride was slightly elevated in MSN mice injected on GD 14 relative to controls (112.8 ± 1.6 mM vs. 109.3 ± 1.2 mM; $p < 0.01$) and glucose was depressed in MSN mice injected on GD 14 relative to controls (176.5 ± 29.7 mg/dL vs. 221.7 ± 19.0 mg/dL; $p < 0.05$). None of the other chemistry blood parameters evaluated were significantly different from controls.

Histopathological Evaluation of Kidneys and Livers

To further evaluate the effect of intravenous MSN administration on liver and kidneys, gravid mice exposed to MSN
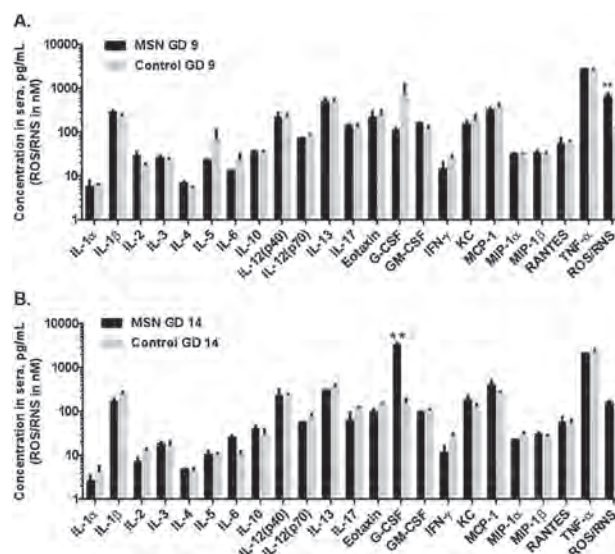
or vehicle alone on GD9 or GD14 were necropsied on GD16. No significant findings were noted by the pathologist in any of the kidney sections examined for either MSN or control group. Findings in the liver varied from mild to moderate microvesicular hepatocellular vacuolation which was often most pronounced in the centrilobular region (Fig. 7). In the MSN mice injected GD14, the vacuolation was more prominent in the portal zones. These findings were moderate and there were no major differences between control animals and treated animals.
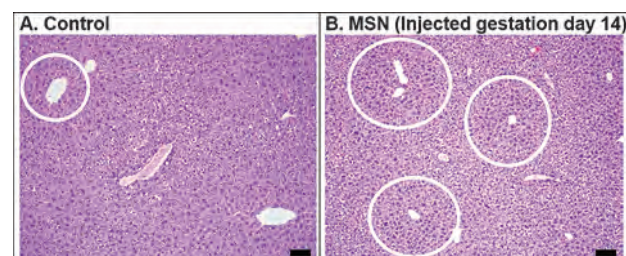

Figure 7. Histopathological findings on livers of gravid mice exposed to MSN during pregnancy. Gravid mice were injected on GD 9 or GD 14 with 0.1 mL saline alone (A) or with 1 mg MSN in 0.1 mL saline (B), livers and kidneys were collected at necropsies on GD16. Livers of gravid mice showed mild to moderate microvesicular hepatocellular vacuolation (circles) regardless of treatment group. Scale bar = 100 μm.

Generally, hepatocyte nuclear vacuolation is considered benign, and in humans, is associated with non-alcohol-related fatty liver disease,[34] or simply due to changes in food intake.[35]

CONCLUSIONS

In this study, we systematically investigated the biocompatibility of novel MSN, first in adherent and non-adherent tissue culture, followed by *in vivo* modeling. The purpose of these investigations is to validate MSN as a minimally-invasive, multimodal tool to model toxicant trafficking. Currently, nanoscale particles are an integral component of numerous engineered particles in industrial and consumer goods. With the increasing exposure to nanoparticles in daily life, it is important to learn more about the potential risks to exposed persons. Following exposure, particles that cross barriers of the skin, lungs, and/or gastrointestinal tract, may gain access to systemic circulation. Upon entering the circulation, because of their size and chemical composition, nanoparticles have access to all organs.[5, 6] A potentially high-vulnerability population to toxicant exposure is pregnant women and developing embryos/fetuses. A number of toxicants such as chemical pesticides, alcohol, narcotics, and the byproducts of cigarette smoke, are known to cross the placental barrier and affect fetal development.[16, 36–38]

Another important aspect is the ever-expanding list of potential applications of nanoparticles as biomedical tools. In the medical field, bioactive chemicals, contrast agents and particulate antitumor agents are often used therapeutically, so expanded study of nanoparticles in the circulation is warranted.[2, 39] Current exposure studies in lab animals typically involve organ and tissue sectioning and assays at a number of time points, and lack real-time *in vivo* analysis. In addition, while previously published works describe the inflammatory response induced by inhaled silica nanoparticles,[6] less is known about the particles when injected systemically.

In advance of studies of toxicants carried in MSN, MSN alone must first be well-characterized as to potential toxicity. The components of the particles have all been evaluated to varying degrees. Amorphous silica nanoparticles have been shown to be biocompatible in cell culture[40] and have a lethal dose (murine i.v. LD_{50}) of over 250 mg/kg.[41] This equates to a dose over an order of magnitude higher than any we have injected. Gadolinium chelates are widely used clinically as MRI contrast agents except for patients with renal disease, and gadolinium oxide nanoparticles are well-tolerated in animals.[17, 42] Poly(ethylene glycol) is biocompatible[43] and used in the digestive system as a mild laxative, and fluorophores such as FITC and TRITC are used *in vivo* to highlight structures for surgical removal, among other uses.[44, 45] However, the combination of these components into one material is novel, and not yet characterized for biocompatibility. Thus, we demonstrated the biocompatibility of the particles by a number of *in vitro* and *in vivo* analyses.

To evaluate toxicity and tagging capability of the particles on adherent and non-adherent cells, we tested various chemical configurations of MSN exposures to cells with dissimilar growth requirements. For example, cell lines tested include several adherence-dependent cell lines: hMSCs,[46, 47] NIH3T3 murine embryonic fibroblasts,[48] H4IIE murine hepatoma,[49] and MB49 murine bladder cancer cells.[50, 51] In addition, non-adherent murine iPSCs were tested.[52] Initial studies used FITC-MSN, Fe_3O_4-MSN and Fe_3O_4-FITC-MSN configurations; additional particle configurations included MSN capped with Gd_2O_3, bismuth, or gold. The uptake of FITC-MSN by hMSCs is shown. Consistently, we observed a minimum adverse effect on cell viability for MSN concentrations from 100–150 μg/mL for each cell type and particle configuration. Other groups have reported similar values for similar particles and cell types.[17, 53] Thus, subsequent experiments were conducted using a particle concentration of 125 μg/mL in growth media.

The intracellular trafficking of particles was documented, first as particles became adherent to the cell membranes, and ultimately as particles were engulfed and compartmentalized in the cells over several days. In the various conditions, particles did not elicit cell stress or adversely affected cell function. The doubling time of normal cells is 2 days, non-labeled and labelled were comparable to published results with similar cell types.[47] Within the first 1–2 days, nearly all the cells were labeled, and very few free particles were observed outside the cells. Thus, once the particles were in the cells, they were well-tolerated during the experiment. Cell division continued consistently until contact inhibition occurred at day 10. Labeled cells that were passaged continued normal division; with each subsequent division, the particles became more dilute and difficult to detect above threshold fluorescence values.

Due to molecular differences in the composition of the bilayer external membrane, compared to anchorage-dependent cells, many non-adherent cells have less reactive membranes and are therefore more difficult to label.[54] In our murine bone marrow transplantation studies, iPSCs stimulated for bone marrow production[52] were exposed to PEG-CF_3-TRITC-Gd_2O_3-MSN. Cell culture media was supplemented with protamine sulfate to improve labeling; these polycationic supplements have long been used to improve uptake for viral transduction.[55] Cell viability appeared to be slightly hindered by MSN exposure, while this effect was mitigated by protamine sulfate supplementation. Wright stains on labeled and non-labeled iPSCs showed a similar phenotype: the majority of cells were found to be progenitors, as determined by their high ratio of nuclear to cytoplasmic volume, while a few cells were found to be more granulocytic in appearance, the proportion of which did not significantly change after

exposure to particles. Thus, binding and uptake with MSN had no significant phenotypic effect on the cells. This is further supported by the flow cytometry data; while it has been observed that the GFP reporter gene grows dimmer as iPSCs differentiate towards granulocytes,[56] we did not observe any shifts in the GFP intensity throughout our exposure studies.

When evaluating the biocompatibility of the MSN, it is important to address the mechanism of uptake in addition to noting viability and phenotypic changes, as each uptake pathway will have a different intracellular fate. These particles do not possess any specific receptor ligands, so the mechanism is unlikely to be a form of receptor-mediated endocytosis. Studies with similar particles have shown evidence for non-specific pinocytosis,[7] while others describe endocytosis via clathrin-coated pits.[3] The fact that protamine sulfate supplementation improves binding supports the involvement of clathrin-coated pits.[57] The intracellular fate of pinocytosed or non-specifically endocytosed cells is essentially the same: vesicle formation followed by fusion with lysosomes as the cell attempts to clear the debris. Other groups have provided evidence for fusion with lysosomes in similar particles, using the combined fluorescence of particles containing fluorophores and fluorescent lysosome tracking reagents.[44] Future studies will investigate the exploitation of specific receptor-mediated endocytosis pathways through the functionalization of the particle surface with ligands for known surface receptors on cells of interest.

In addition to the demonstration of viability at the cellular level, it is important to analyze systemic responses to particulate exposure. Here, the mode of exposure has a great effect on the systemic response. Similar silica nanoparticles have been shown to induce inflammatory cascades in an inhalation model,[6] while i.v.-injected particles are tolerated at very high doses.[41] The former more closely models an environmental exposure while the latter represents a therapeutic route. Furthermore, while inhalation is a good option for studies of the effects of particulates in the air, it has limitations. First, the amount of material inhaled and transiting to the bloodstream is difficult to precisely measure. In addition, the quality of the compounds may be altered at the pulmonary barrier prior to uptake. After they cross the barrier, particles become diluted and are difficult to trace in the absence of a moiety that provides fluorescence or imaging contrast.

Therefore, in this study, we examined the effects of MSN following systemic injection, using two models. In the first, particles were injected systemically using a retro-orbital approach in a murine model for bone marrow transplant. This model is beneficial for studying biocompatibility because it is well-established,[52] it allows for the *in vivo* tracking of labeled cells in addition to free MSN, and it represents another clinically relevant scenario in which the MSN can be utilized. Hypointensities observed

at the injection site and later in the kidney vasculature indicate the MSN are cleared via renal pathways. Our observations are consistent with similar studies involving intravenous injection of NPs of various sizes. Some studies have shown a slowing of renal clearance for particles as small as 10 nm;[58] however, this study was conducted using quantum dots, which are known toxicants.[59] Other studies with well-characterized biocompatible particles show renal clearance for sizes up to 100 nm,[27] and hepatic/digestive clearance for larger particles.[60]

Subsequently, we followed various parameters in the injected mice, including signal changes in the spleen and bone marrow, with no observed co-morbidity. MRI scans were carried out for 21 days after tail vein injection, and mice were observed for adverse reactions for 42 days after injection. Of 10 total mice, 5 were sacrificed at day 21 and 4 were monitored until day 42, and one died during the injection procedure. Despite sonication, agglomerated MSN were observed in that sample; thus, extra care was taken to ensure a monodisperse, small (less than 200 nm) particle size prior to carrying out subsequent injections. Furthermore, subsequent injections carried out in gravid mice used a tail vein approach; this reduced the chance of a particle aggregate traveling directly to the brain. Overall, our observations are consistent with those that show a high tolerance of silica-based particles *in vivo*.[60]

Despite the importance of the placenta in fetal development, its total functions are not well-characterized. Although it has long been known for the maternal-fetal transfer of dissolved gases, nutrients, and other small molecules, only recently has it been discovered to have exocrine effects on the fetus, secreting a number of growth factors and other hormones.[61] Similarly, the trans-placental transport of other, larger molecules and particles, including toxicants, has not been well-characterized. In part, this is due to the difficulty of studying the placenta in real-time; although animal studies have been carried out, access to human placenta is limited. In order to address these issues, we have developed our MSN contrast agents for multimodal, real-time quantification of trans-placental trafficking.

To understand the effects of nanoparticles on fetal development, gravid mice were injected with 1 mg PEG-CF$_3$-TRITC-Gd$_2$O$_3$-MSN, or saline as a control, using a tail vein approach for systemic injections at varying points during gestation. The dose of 1 mg was chosen specifically because of its clinical relevance; this quantity is sufficient to produce observable contrast in MRI, but orders of magnitude below the known LD$_{50}$ for amorphous silica in mice.[41] The timing of the injections was chosen to represent early/mid gestation (6–9 days), or late gestation (15–16 days). Based on Carnegie staging, these injections corresponded to 13–20 days and 54–58 days of human gestation, respectively.[62] During early/mid gestation, the primitive heart and neural plate are developing, and somites develop on day 8–9 in the mouse. By GD 16 in the mouse,

the embryo is nearly fully formed. In human gestation, week 8 is considered the end of embryonic development and the beginning of fetal development, as the organs and tissues are present largely in their final morphology.

Throughout gestation, the maternal body weights were monitored, and the fetuses and placentas were scanned with MRI and ultrasound imaging. In similar animal studies, adverse reactions to toxicants present as poor weight gain in the mothers, spontaneous resorptions and/or stillborn fetuses, and lower than normal weights in fetuses were found.[63] Here, we saw no significant differences in maternal weight during gestation, or in maternal organs after necropsy. A follow up post mortem investigation of fetuses and placentas revealed that litter sizes and the number of spontaneous resorptions and underdeveloped fetuses were similar in MSN-exposed mice and controls. Although spontaneous embryo resorption is relatively uncommon in humans, it has been documented as relatively common in mice using high frequency ultrasound,[33] and in livestock animals it has significant economic consequences. Generally, spontaneous embryo resorption reflects a complex underlying mechanism including chromosomal anomalies, placental insufficiency, and disturbances in the maternal-fetal barrier.[32]

Typically, studies of effects of toxicants on gestational development are concerned with embryos having a lower weight due to underdevelopment.[64] However, changes in embryonic weight alone are insufficient to determine the adverse effect of a toxicant; as weight can vary greatly among individual mice in a population regardless of treatment.[65] For example, animal studies of inhaled diesel exhaust can be associated with either an increase[66–68] or decrease[69,70] in embryonic, placental, or neonatal body weight. In our study, embryos and placentas exposed to particles during early-mid gestation (GD 9) were slightly underweight relative to controls, but not to a statistically significant level (Table II). Conversely, the embryos and placentas exposed to particles during late gestation (GD 14) were slightly above weight relative to their control counterparts; the placentas were 42.3% larger ($p < 0.01$), while the embryos were 17.6% larger ($p < 0.05$). If there exists a causal link between late-gestational MSN exposure and increased embryonic weight, the mechanism by which this occurs is unclear. The aforementioned diesel studies associate the increased embryonic weight with increased production of inflammatory proteins, in addition to a much higher rate of spontaneous embryonic resorptions and developmental issues[67] that we did not observe in MSN-exposed pups that were carried to term. To further support our hypothesis, maternal livers and sera were collected at the time of necropsy and tested for an array of inflammatory cytokines and ROS/RNS. Inflammatory reactions to injected particles typically involve the interleukin (IL) family, interferon-gamma (IFN-γ), and/or tumor necrosis factor alpha (TNF-α).[71] The only cytokine which showed a significantly different concentration in MSN-exposed mice relative to controls was G-CSF, and only in mice injected during late gestation. An elevated level of G-CSF in MSN-exposed animals is expected, as G-CSF is a known stimulator of the production of neutrophils, which clear various debris from tissue.[72] G-CSF has also been found to have beneficial effects, including neuroprotection;[72] this, in conjunction with the fact that more potent inflammatory cytokines (IL/IFN-γ/TNF-α) were not elevated, even in mice injected earlier in gestation, allowing more time for a reaction to take place, suggest a low level of maternal reaction to the MSN.

Interestingly, although pregnant mice exposed to MSN during early gestation did not show elevated cytokine levels, they did show elevated levels of ROS/RNS in the maternal sera. Luo et al., showed a similar increase by cultured macrophages 24–48 hours after exposure to MSN, an effect which was mitigated by coating the particles with biocompatible hydrogel, albumin, or lysine.[71] Typically, high levels of ROS can lead to chronic inflammation,[73] though here the ROS/RNS increase does not appear to be associated with an increase in interleukin or interferon activity, and histopathology of liver showed only mild accumulation of neutrophils, eosinophils, and macrophages in both control and MSN-exposed mice. The reason for this is unclear, though it may be related to the timing of injections and necropsies. In another example of chronic inflammation, a mouse model for colitis takes up to 4 weeks between stimulation with non-steroidal anti-inflammatory drug treatment and the onset of symptoms.[74] Thus, the 7 days between injection and necropsy may be too limited to observe a chronic inflammatory response. Histopathology evaluation of kidneys found no significant pathologies. The absence of pathology in livers was supported by no significant findings of major liver enzymes in plasma of MSN-treated mice such as ALP, ALT, and AST. Furthermore, normal kidney function was supported by a lack of elevation of BUN, creatinine or total bilirubin in the plasma of MSN-treated mice.

Data presented herein strongly confirm the relatively inert nature of systemic MSN. In cultured cells no significant adverse effects were seen on cell viability at concentrations in growth media up to 125 μg/mL, and *in vivo* models demonstrated minimal acute responses. In addition, future studies will make use of the MSN as a biocompatible tool for non-invasive, real-time tracking of cells or particles in live experiments. In the mouse model for bone marrow transplant, we will use the particles to label hematopoietic progenitor cells, using MRI to measure homing of cells to the bone marrow. Under the current approach, the use of a GFP reporter gene to detect implantation via chimerism in the blood takes up to 6 weeks. With a novel approach using MRI detection of implantation, analysis delays can be reduced significantly. Additionally, the particles will be used in future studies of transplacental transport, in order to gain insight into the effect of size- and time-dependence on transport into the

fetus. The unique ability to visualize the particles using MRI, including in the placenta, can be of great benefit to the study of the as-yet unknown properties of the placenta.

Competing Interests

Jose G. Assouline is founder and sole proprietor of NanoMedTrix, LLC, which prepared the nanoparticles used in this study. All results and claims have been independently verified by other scientists with no financial stake in the company.

REFERENCES

1. J. S. Valenstein, K. Kandel, F. Melcher, I. I. Slowing, V. S. Lin, and B. G. Trewyn, Functional mesoporous silica nanoparticles for the selective sequestration of free fatty acids from microalgal oil. *ACS Appl. Mater. Interfaces* 4, 1003 (**2012**).
2. Y. Zhao, X. Sun, G. Zhang, B. G. Trewyn, I. I. Slowing, and V. S. Lin, Interaction of mesoporous silica nanoparticles with human red blood cell membranes: Size and surface effects. *ACS Nano* 5, 1366 (**2011**).
3. I. J. Fang, I. I. Slowing, K. C. Wu, V. S. Lin, and B. G. Trewyn, Ligand conformation dictates membrane and endosomal trafficking of arginine-glycine-aspartate (RGD)-functionalized mesoporous silica nanoparticles. *Chemistry* 18, 7787 (**2012**).
4. A. Abbaszad Rafi, M. Mahkam, S. Davaran, and H. Hamishehkar, A smart pH-responsive nano-carrier as a drug delivery system: A hybrid system comprised of mesoporous nanosilica MCM-41 (as a nano-container) and a pH-sensitive polymer (as smart reversible gatekeepers): Preparation, characterization and *in vitro* release studies of an anti-cancer drug. *Eur. J. Pharm. Sci.* 93, 64 (**2016**).
5. M. Schneider, F. Stracke, S. Hansen, and U. F. Schaefer, Nanoparticles and their interactions with the dermal barrier. *Dermatoendocrinol.* 1, 197 (**2009**).
6. T. Yoshida, Y. Yoshioka, S. Tochigi, T. Hirai, M. Uji, K. Ichihashi, K. Nagano, Y. Abe, H. Kamada, S. Tsunoda, H. Nabeshi, K. Higashisaka, T. Yoshikawa, and Y. Tsutsumi, Intranasal exposure to amorphous nanosilica particles could activate intrinsic coagulation cascade and platelets in mice. *Part Fibre Toxicol.* 10, 41-8977-10-41 (**2013**).
7. E. W. Carney, A. R. Scialli, R. E. Watson, and J. M. DeSesso, Mechanisms regulating toxicant disposition to the embryo during early pregnancy: An interspecies comparison. *Birth Defects Res. C. Embryo. Today* 72, 345 (**2004**).
8. M. Chu, Q. Wu, H. Yang, R. Yuan, S. Hou, Y. Yang, Y. Zou, S. Xu, K. Xu, A. Ji, and L. Sheng, Transfer of quantum dots from pregnant mice to pups across the placental barrier. *Small* 6, 670 (**2010**).
9. S. Correia Carreira, L. Walker, K. Paul, and M. Saunders, The toxicity, transport and uptake of nanoparticles in the *in vitro* BeWo b30 placental cell barrier model used within NanoTEST. *Nanotoxicology* 9, 66 (**2015**).
10. S. Grafmueller, P. Manser, L. Diener, P. A. Diener, X. Maeder-Althaus, L. Maurizi, W. Jochum, H. F. Krug, T. Buerki-Thurnherr, U. von Mandach, and P. Wick, Bidirectional transfer study of polystyrene nanoparticles across the placental barrier in an *ex vivo* human placental perfusion model. *Environ. Health Perspect.* 123, 1280 (**2015**).
11. M. Bobak, Outdoor air pollution, low birth weight, and prematurity. *Environ. Health Perspect.* 108, 173 (**2000**).
12. S. Kannan, D. P. Misra, J. T. Dvonch, and A. Krishnakumar, Exposures to airborne particulate matter and adverse perinatal outcomes: A biologically plausible mechanistic framework for exploring potential effect modification by nutrition. *Environ. Health Perspect.* 114, 1636 (**2006**).
13. S. Takenaka, E. Karg, C. Roth, H. Schulz, A. Ziesenis, U. Heinzmann, P. Schramel, and J. Heyder, Pulmonary and systemic distribution of inhaled ultrafine silver particles in rats. *Environ. Health Perspect.* 109(Suppl 4), 547 (**2001**).
14. A. Nemmar, P. H. Hoet, B. Vanquickenborne, D. Dinsdale, M. Thomeer, M. F. Hoylaerts, H. Vanbilloen, L. Mortelmans, and B. Nemery, Passage of inhaled particles into the blood circulation in humans. *Circulation* 105, 411 (**2002**).
15. A. Sood, S. Salih, D. Roh, L. Lacharme-Lora, M. Parry, B. Hardiman, R. Keehan, R. Grummer, E. Winterhager, P. J. Gokhale, P. W. Andrews, C. Abbott, K. Forbes, M. Westwood, J. D. Aplin, E. Ingham, I. Papageorgiou, M. Berry, J. Liu, A. D. Dick, R. J. Garland, N. Williams, R. Singh, A. K. Simon, M. Lewis, J. Ham, L. Roger, D. M. Baird, L. A. Crompton, M. A. Caldwell, H. Swalwell, M. Birch-Machin, G. Lopez-Castejon, A. Randall, H. Lin, M. S. Suleiman, W. H. Evans, R. Newson, and C. P. Case, Signalling of DNA damage and cytokines across cell barriers exposed to nanoparticles depends on barrier thickness. *Nat. Nanotechnol.* 6, 824 (**2011**).
16. K. Yamashita, Y. Yoshioka, K. Higashisaka, K. Mimura, Y. Morishita, M. Nozaki, T. Yoshida, T. Ogura, H. Nabeshi, K. Nagano, Y. Abe, H. Kamada, Y. Monobe, T. Imazawa, H. Aoshima, K. Shishido, Y. Kawai, T. Mayumi, S. Tsunoda, N. Itoh, T. Yoshikawa, I. Yanagihara, S. Saito, and Y. Tsutsumi, Silica and titanium dioxide nanoparticles cause pregnancy complications in mice. *Nat. Nanotechnol.* 6, 321 (**2011**).
17. J. K. Hsiao, C. P. Tsai, T. H. Chung, Y. Hung, M. Yao, H. M. Liu, C. Y. Mou, C. S. Yang, Y. C. Chen, and D. M. Huang, Mesoporous silica nanoparticles as a delivery system of gadolinium for effective human stem cell tracking. *Small* 4, 1445 (**2008**).
18. M. Benezra, O. Penate-Medina, P. B. Zanzonico, D. Schaer, H. Ow, A. Burns, E. DeStanchina, V. Longo, E. Herz, S. Iyer, J. Wolchok, S. M. Larson, U. Wiesner, and M. S. Bradbury, Multimodal silica nanoparticles are effective cancer-targeted probes in a model of human melanoma. *J. Clin. Invest.* 121, 2768 (**2011**).
19. Y. Chen, H. Chen, D. Zeng, Y. Tian, F. Chen, J. Feng, and J. Shi, Core/shell structured hollow mesoporous nanocapsules: A potential platform for simultaneous cell imaging and anticancer drug delivery. *ACS Nano* 4, 6001 (**2010**).
20. N. Z. Knezevic, B. G. Trewyn, and V. S. Lin, Light- and pH-responsive release of doxorubicin from a mesoporous silica-based nanocarrier. *Chemistry* 17, 3338 (**2011**).
21. S. K. Sweeney, Y. Luo, M. A. O'Donnell, and J. Assouline, Nanotechnology and cancer: Improving real-time monitoring and staging of bladder cancer with multimodal mesoporous silica nanoparticles. *Cancer Nanotechnol.* 7, 3 (**2016**).

22. R. M. Samsonraj, B. Rai, P. Sathiyanathan, K. J. Puan, O. Rotzschke, J. H. Hui, M. Raghunath, L. W. Stanton, V. Nurcombe, and S. M. Cool, Establishing criteria for human mesenchymal stem cell potency. *Stem Cells* 33, 1878 (**2015**).

23. C. Wilhelm, F. Gazeau, J. Roger, J. N. Pons, and J. Bacri, Interaction of anionic superparamagnetic nanoparticles with cells:‰ kinetic analyses of membrane adsorption and subsequent internalization. *Langmuir* 18, 8148 (**2002**).

24. H. J. Jin, Y. K. Bae, M. Kim, S. J. Kwon, H. B. Jeon, S. J. Choi, S. W. Kim, Y. S. Yang, W. Oh, and J. W. Chang, Comparative analysis of human mesenchymal stem cells from bone marrow, adipose tissue, and umbilical cord blood as sources of cell therapy. *Int. J. Mol. Sci.* 14, 17986 (**2013**).

25. X. Sun, Y. Zhao, V. S. Lin, I. I. Slowing, and B. G. Trewyn, Luciferase and luciferin co-immobilized mesoporous silica nanoparticle materials for intracellular biocatalysis. *J. Am. Chem. Soc.* 133, 18554 (**2011**).

26. G. F. Luo, W. H. Chen, Y. Liu, Q. Lei, R. X. Zhuo, and X. Z. Zhang, Multifunctional enveloped mesoporous silica nanoparticles for subcellular co-delivery of drug and therapeutic peptide. *Sci. Rep.* 4, 6064 (**2014**).

27. J. L. Vivero-Escoto, K. M. Taylor-Pashow, R. C. Huxford, J. Della Rocca, C. Okoruwa, H. An, W. Lin, and W. Lin, Multifunctional mesoporous silica nanospheres with cleavable Gd(III) chelates as MRI contrast agents: Synthesis, characterization, target-specificity, and renal clearance. *Small* 7, 3519 (**2011**).

28. L. T. Sa, S. Albernaz Mde, B. F. Patricio, M. V. Falcao, Jr., B. F. Coelho, A. Bordim, J. C. Almeida, and R. Santos-Oliveira, Biodistribution of nanoparticles: Initial considerations. *J. Pharm. Biomed. Anal.* 70, 602 (**2012**).

29. F. Chen, H. Hong, Y. Zhang, H. F. Valdovinos, S. Shi, G. S. Kwon, C. P. Theuer, T. E. Barnhart, and W. Cai, *In vivo* tumor targeting and image-guided drug delivery with antibody-conjugated, radiolabeled mesoporous silica nanoparticles. *ACS Nano* 7, 9027 (**2013**).

30. F. Chen, H. Hong, S. Goel, S. A. Graves, E. B. Ehlerding, S. Shi, C. P. Theuer, R. J. Nickles, and W. Cai, *In vivo* tumor vasculature targeting of CuS@MSN based theranostic nanomedicine. *ACS Nano* 9, 3926 (**2015**).

31. Y. Tang, C. Zhang, J. Wang, X. Lin, L. Zhang, Y. Yang, Y. Wang, Z. Zhang, J. W. Bulte, and G. Y. Yang, MRI/SPECT/Fluorescent trimodal probe for evaluating the homing and therapeutic efficacy of transplanted mesenchymal stem cells in a rat ischemic stroke model. *Adv. Funct. Mater.* 25, 1024 (**2015**).

32. A. C. Zenclussen, K. Gerlof, M. L. Zenclussen, A. Sollwedel, A. Z. Bertoja, T. Ritter, K. Kotsch, J. Leber, and H. D. Volk, Abnormal T-cell reactivity against paternal antigens in spontaneous abortion: Adoptive transfer of pregnancy-induced CD4+CD25+T regulatory cells prevents fetal rejection in a murine abortion model. *Am. J. Pathol.* 166, 811 (**2005**).

33. L. E. Flores, T. B. Hildebrandt, A. Kühl A, and B. Drews, Early detection and staging of spontaneous embryo resorption by ultrasound biomicroscopy in murine pregnancy. *Reproductive Biology and Endocrinology: RB&E* 12, 38 (**2014**).

34. A. Aravinthan, S. Verma, N. Coleman, S. Davies, M. Allison, and G. Alexander, Vacuolation in hepatocyte nuclei is a marker of senescence. *J. Clin. Pathol.* 65, 557 (**2012**).

35. E. Ulusoy and B. Eren, Histological changes on liver glycogen storage in mice (Mus musculus) caused by unbalanced diets. *Clin. Med. Pathol.* 1, 69 (**2008**).

36. K. S. Hougaard, P. Jackson, K. A. Jensen, J. J. Sloth, K. Loschner, E. H. Larsen, R. K. Birkedal, A. Vibenholt, A. M. Boisen, H. Wallin, and U. Vogel, Effects of prenatal exposure to surface-coated nano-sized titanium dioxide (UV-Titan). *A Study in Mice. Part Fibre Toxicol.* 7, 16-8977-7-16 (**2010**).

37. J. Veid, V. Karttunen, K. Myohanen, P. Myllynen, S. Auriola, T. Halonen, and K. Vahakangas, Acute effects of ethanol on the transfer of nicotine and two dietary carcinogens in human placental perfusion. *Toxicol. Lett.* 205, 257 (**2011**).

38. M. Heller and L. Burd, Review of ethanol dispersion, distribution, and elimination from the fetal compartment. *Birth Defects Res. A. Clin. Mol. Teratol.* 100, 277 (**2014**).

39. I. Slowing, B. G. Trewyn, and V. S. Lin, Effect of surface functionalization of MCM-41-type mesoporous silica nanoparticles on the endocytosis by human cancer cells. *J. Am. Chem. Soc.* 128, 14792 (**2006**).

40. J. Duan, Y. Yu, Y. Li, Y. Yu, Y. Li, X. Zhou, P. Huang, and Z. Sun, Toxic effect of silica nanoparticles on endothelial cells through DNA damage response via Chk1-dependent G2/M checkpoint. *PLoS One* 8, e62087 (**2013**).

41. Y. Yu, Y. Li, W. Wang, M. Jin, Z. Du, Y. Li, J. Duan, Y. Yu, and Z. Sun, Acute toxicity of amorphous silica nanoparticles in intravenously exposed ICR mice. *PLoS One* 8, e61346 (**2013**).

42. J. L. Bridot, A. C. Faure, S. Laurent, C. Riviere, C. Billotey, B. Hiba, M. Janier, V. Josserand, J. L. Coll, L. V. Elst, R. Muller, S. Roux, P. Perriat, and O. Tillement, Hybrid gadolinium oxide nanoparticles: Multimodal contrast agents for *in vivo* imaging. *J. Am. Chem. Soc.* 129, 5076 (**2007**).

43. G. Kaul and M. Amiji, Cellular interactions and *in vitro* DNA transfection studies with poly(ethylene glycol)-modified gelatin nanoparticles. *J. Pharm. Sci.* 94, 184 (**2005**).

44. D. M. Huang, Y. Hung, B. S. Ko, S. C. Hsu, W. H. Chen, C. L. Chien, C. P. Tsai, C. T. Kuo, J. C. Kang, C. S. Yang, C. Y. Mou, and Y. C. Chen, Highly efficient cellular labeling of mesoporous nanoparticles in human mesenchymal stem cells: Implication for stem cell tracking. *FASEB J.* 19, 2014 (**2005**).

45. G. M. van Dam, G. Themelis, L. M. Crane, N. J. Harlaar, R. G. Pleijhuis, W. Kelder, A. Sarantopoulos, J. S. de Jong, H. J. Arts, A. G. van der Zee, J. Bart, P. S. Low, and V. Ntziachristos, Intraoperative tumor-specific fluorescence imaging in ovarian cancer by folate receptor-alpha targeting: First in-human results. *Nat. Med.* 17, 1315 (**2011**).

46. P. J. Simmons and B. Torok-Storb, Identification of stromal cell precursors in human bone marrow by a novel monoclonal antibody, STRO-1. *Blood* 78, 55 (**1991**).

47. G. D'Ippolito, S. Diabira, G. A. Howard, P. Menei, B. A. Roos, and P. C. Schiller, Marrow-isolated adult multilineage inducible (MIAMI) cells, a unique population of postnatal young and old human cells with extensive expansion and differentiation potential. *J. Cell. Sci.* 117, 2971 (**2004**).

48. K. A. Westerman and P. Leboulch, Reversible immortalization of mammalian cells mediated by retroviral transfer and site-specific recombination. *Proc. Natl. Acad. Sci. U.S.A.* 93, 8971 (**1996**).

49. H. C. Pitot, C. Peraino, P. A. Morse, Jr., and V. R. Potter, Hepatomas in tissue culture compared with adapting liver *in vivo*. *Natl. Cancer Inst. Monogr.* 13, 229 (**1964**).

50. I. C. Summerhayes and L. M. Franks, Effects of donor age on neoplastic transformation of adult mouse bladder epithelium *in vitro*. *J. Natl. Cancer Inst.* 62, 1017 (**1979**).

51. Y. Luo and M. J. Knudson, Mycobacterium bovis bacillus calmette-guerin-induced macrophage cytotoxicity against bladder cancer cells. *Clin. Dev. Immunol.* 2010, 357591 (**2010**).

52. W. B. Tabayoyong, J. G. Salas, S. Bonde, and N. Zavazava, HOXB4-transduced embryonic stem cell-derived Lin-c-kit+ and Lin-Sca-1+ hematopoietic progenitors express H60 and are targeted by NK cells. *J. Immunol.* 183, 5449 (**2009**).

53. P. J. Kempen, S. Greasley, K. A. Parker, J. L. Campbell, H. Y. Chang, J. R. Jones, R. Sinclair, S. S. Gambhir, and J. V. Jokerst, Theranostic mesoporous silica nanoparticles biodegrade after pro-survival drug delivery and ultrasound/magnetic resonance imaging of stem cells. *Theranostics* 5, 631 (**2015**).

54. B. Janic, A. M. Rad, E. K. Jordan, A. S. Iskander, M. M. Ali, N. R. Varma, J. A. Frank, and A. S. Arbab, Optimization and validation of FePro cell labeling method. *PLoS One* 4, e5873 (**2009**).

55. K. Cornetta and W. F. Anderson, Protamine sulfate as an effective alternative to polybrene in retroviral-mediated gene-transfer: Implications for human gene therapy. *J. Virol. Methods* 23, 187 **(1989)**.

56. C. Christodoulou, T. A. Longmire, S. S. Shen, A. Bourdon, C. A. Sommer, P. Gadue, A. Spira, V. Gouon-Evans, G. J. Murphy, G. Mostoslavsky, and D. N. Kotton, Mouse ES and iPS cells can form similar definitive endoderm despite differences in imprinted genes. *J. Clin. Invest.* 121, 2313 **(2011)**.

57. D. Delgado, A. del Pozo-Rodriguez, M. A. Solinis, and A. Rodriguez-Gascon, Understanding the mechanism of protamine in solid lipid nanoparticle-based lipofection: The importance of the entry pathway. *Eur. J. Pharm. Biopharm.* 79, 495 **(2011)**.

58. H. S. Choi, W. Liu, P. Misra, E. Tanaka, J. P. Zimmer, B. Itty Ipe, M. G. Bawendi, and J. V. Frangioni, Renal clearance of quantum dots. *Nat. Biotechnol.* 25, 1165 **(2007)**.

59. T. Liu, R. Xing, Y. F. Zhou, J. Zhang, Y. Y. Su, K. Q. Zhang, Y. He, Y. H. Sima, and S. Q. Xu, Hematopoiesis toxicity induced by CdTe quantum dots determined in an invertebrate model organism. *Biomaterials* 35, 2942 **(2014)**.

60. T. Liu, L. Li, X. Teng, X. Huang, H. Liu, D. Chen, J. Ren, J. He, and F. Tang, Single and repeated dose toxicity of mesoporous hollow silica nanoparticles in intravenously exposed mice. *Biomaterials* 32, 1657 **(2011)**.

61. M. R. Du, S. C. Wang, and D. J. Li, The integrative roles of chemokines at the maternal-fetal interface in early pregnancy. *Cell. Mol. Immunol.* 11, 438 **(2014)**.

62. M. A. Hill, Early human development. *Clin. Obstet. Gynecol.* 50, 2 **(2007)**.

63. P. E. Mullis and P. Tonella, Regulation of fetal growth: Consequences and impact of being born small. *Best Pract. Res. Clin. Endocrinol. Metab.* 22, 173 **(2008)**.

64. K. S. Hougaard, L. Campagnolo, P. Chavatte-Palmer, A. Tarrade, D. Rousseau-Ralliard, S. Valentino, M. V. Park, W. H. de Jong, G. Wolterink, A. H. Piersma, B. L. Ross, G. R. Hutchison, J. S. Hansen, U. Vogel, P. Jackson, R. Slama, A. Pietroiusti, and F. R. Cassee, A perspective on the developmental toxicity of inhaled nanoparticles. *Reprod. Toxicol.* 56, 118 **(2015)**.

65. M. A. van Engelen, M. K. Nielsen, and E. L. Ribeiro, Differences in pup birth weight, pup variability within litters, and dam weight of mice selected for alternative criteria to increase litter size. *J. Anim. Sci.* 73, 1948 **(1995)**.

66. N. Watanabe and M. Kurita, The masculinization of the fetus during pregnancy due to inhalation of diesel exhaust. *Environ. Health Perspect.* 109, 111 **(2001)**.

67. A. Fujimoto, N. Tsukue, M. Watanabe, I. Sugawara, R. Yanagisawa, H. Takano, S. Yoshida, and K. Takeda, Diesel exhaust affects immunological action in the placentas of mice. *Environ. Toxicol.* 20, 431 **(2005)**.

68. C. Li, X. Li, A. K. Suzuki, Y. Zhang, Y. Fujitani, K. Nagaoka, G. Watanabe, and K. Taya, Effects of exposure to nanoparticle-rich diesel exhaust on pregnancy in rats. *J. Reprod. Dev.* 59, 145 **(2013)**.

69. N. Watanabe and M. Ohsawa, Elevated serum immunoglobulin E to Cryptomeria japonica pollen in rats exposed to diesel exhaust during fetal and neonatal periods. *BMC Pregnancy Childbirth* 2, 2 **(2002)**.

70. C. S. Weldy, Y. Liu, H. D. Liggitt, and M. T. Chin, In utero exposure to diesel exhaust air pollution promotes adverse intrauterine conditions, resulting in weight gain, altered blood pressure, and increased susceptibility to heart failure in adult mice. *PLoS One* 9, e88582 **(2014)**.

71. Z. Luo, Y. Hu, R. Xin, B. Zhang, J. Li, X. Ding, Y. Hou, L. Yang, and K. Cai, Surface functionalized mesoporous silica nanoparticles with natural proteins for reduced immunotoxicity. *J. Biomed. Mater. Res. A* 102, 3781 **(2014)**.

72. I. Solaroglu, J. Cahill, V. Jadhav, and J. H. Zhang, A novel neuroprotectant granulocyte-colony stimulating factor. *Stroke* 37, 1123 **(2006)**.

73. H. Ahsan, A. Ali, and R. Ali, Oxygen free radicals and systemic autoimmunity. *Clin. Exp. Immunol.* 131, 398 **(2003)**.

74. D. J. Berg, J. Zhang, J. V. Weinstock, H. F. Ismail, K. A. Earle, H. Alila, R. Pamukcu, S. Moore, and R. G. Lynch, Rapid development of colitis in NSAID-treated IL-10-deficient mice. *Gastroenterology* 123, 1527 **(2002)**.